

LASER APPLICATIONS AND OTHER TOPICS IN QUANTUM ELECTRONICS

PACS numbers: 04.80.Nn; 07.60.Ly; 78.20.Ls; 42.25.Ja
DOI: 10.1070/QE2012v042n04ABEH014817

Optical isolation in the LIGO gravitational wave laser detector in transient states

A.A. Soloviev, E.A. Khazanov

Abstract. **This paper presents a numerical analysis of the degree of optical isolation of the laser source by the Faraday isolator in transient states of the laser interferometer gravitational wave observatory (LIGO) detector. This system may be in transient states where the power of the light reflected from the detector to the laser source can exceed many times the power of the source. The present results can be used to analyse the need for installing an additional active mechanical isolation of the source and to evaluate its response time.**

Keywords: *Faraday isolator, transient depolarisation, gravitational wave laser detector.*

1. Introduction

Faraday isolators, with a classic scheme represented in Fig.1a, are basic to no-failure operation of cw and pulsed laser systems and allow one, in principle, to completely rule out damage to the source by the back-reflected light from optical circuit components. At high laser beam powers, however, optical isolation quality is substantially poorer because of the thermal depolarisation, resulting from light absorption in the isolator [1, 2]. To improve isolation quality at a high average power, use is made of various layouts and approaches [2–7]. The most widely used configuration is that described in Refs [2, 8], which comprises two $3\pi/8$ Faraday (nonreciprocal) rotators and one $3\pi/8$ reciprocal rotator, e.g. made of quartz (Fig. 1b). This configuration is attractive in that it is relatively simple and ensures a significant increase in the degree of isolation [9–12]. In particular, it is employed [11, 12] in the LIGO and Virgo interferometer gravitational wave detectors [13–16].

A Faraday isolator incorporated into a particular optical chain must ensure optical isolation of the source from back-reflected light in all possible conditions. In addition to steady-state operation, intended for gravitational wave detection, LIGO has several transient states, in which the heat generation rate and the laser light power back-reflected to the optical isolator are substantially higher than those in the steady state. The reason for this is that the detector includes huge optical cavities (Fig. 2), which accumulate optical energy and, under certain conditions, may direct it back to the laser source. Such transient states are of special interest because they correspond to the highest probability that the laser source will be damaged. At the same time, previous studies of thermal effects in Faraday isolators were limited to steady-state operation [1, 2, 8, 9–12, 17–19]. In this paper, we analyse the efficiency of a Faraday isolator in the optical chain of the LIGO detector in transient states.

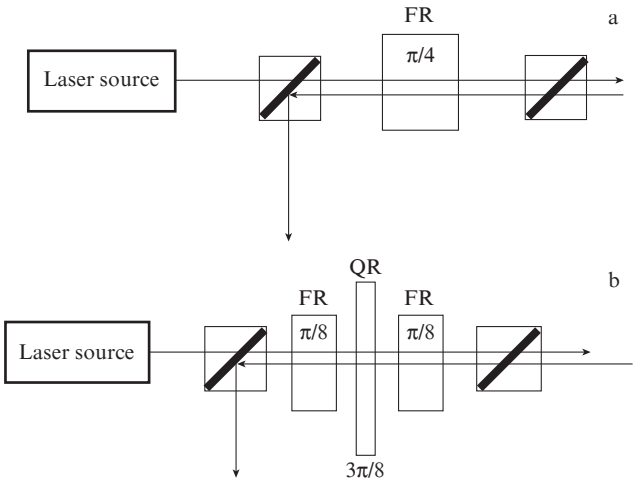

Figure 1. (a) Classic Faraday isolator and (b) configuration with thermal distortion compensation: (FR) Faraday rotator, (QR) quartz reciprocal rotator.

A.A. Soloviev, E.A. Khazanov Institute of Applied Physics, Russian Academy of Sciences, ul. Ul'yanova 46, 603950 Nizhnii Novgorod, Russia; e-mail: so_lo@appl.sci-nnov.ru

Received 24 January 2012
Kvantovaya Elektronika **42** (4) 367–371 (2012)
Translated by O.M. Tsarev

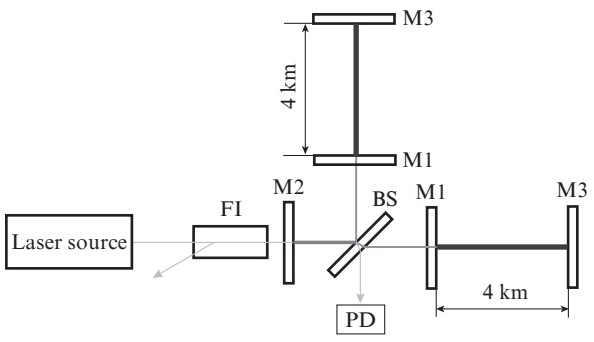

Figure 2. Schematic of the LIGO interferometer gravitational wave detector [13–15]: (FI) Faraday isolator, (BS) beam splitter, (M1) input test mass mirror, (M2) power recycling mirror, (M3) end test mass mirror, (PD) photodetector.

2. Operation regimes of the LIGO interferometer

The LIGO project includes two widely separated detectors similar in design, one located in the State of Washington and the other in Louisiana (USA). Each detector is an enormous Michelson interferometer (Fig. 2) fed with linearly polarised 125-W, 1064-nm light (5-mm beam diameter) through a Faraday isolator. Gravitational waves produced by colossal cosmic events, such as a supernova explosion, merger of neutron stars and star capture by a black hole, are expected to cause minute relative changes ($< 10^{-21}$ [15]) in the length of the interferometer arms and, accordingly, in the output optical signal, measured by a photodetector (PD).

To improve the sensitivity to relative changes in the lengths of the arms, the optical system includes additional elements: input test mass mirror M1 and power recycling mirror M2 (Fig. 2). When the optical cavity formed by the M1 and M3 mirrors is locked (the cavity round-trip path length is then a multiple of the laser wavelength), the power of the light circulating in the cavity is about two orders of magnitude greater than that in a conventional Michelson interferometer because the reflectivity of the end test mass mirror M3 is almost unity. Note that, in the locked state, the behaviour of this cavity with respect to incident light is similar to that of a mirror with a reflectivity of almost unity, but the reflected light is phase-shifted by π.

The cavity formed by the recycling mirror M2 and the Michelson interferometer in the locked state can also be locked, which further increases the laser light power in the interferometer arms. This configuration is referred to as a recycled Fabry–Perot–Michelson interferometer and increases the laser light power in the interferometer arms (and its sensitivity to gravitational waves) by about 8000 times [15], i.e. to about 1 MW. The state in which all the cavities are locked is referred to as normal operation (locked state) in internal working notes of the LIGO project and is the only state in which gravitational waves can be detected because it offers the highest sensitivity to relative changes in the lengths of the arms. In an ideal case, the LIGO interferometer should be kept constantly locked.

However, increasing the laser light power in the cavities to 1 MW leads not only to a higher sensitivity of the interferometer but also to a relatively low stability of the system. Lock loss leads to sequential transitions to regimes A and B (Table 1). Because of the thermal effects in M2, BS, M1 and M3, a complex, multistep procedure is needed to lock the system (state C).

In the locked state, the wave reflected from M2 and that transmitted through M2 in the backward direction differ in phase by $\Delta\varphi = \pi$, which leads to destructive interference of the waves and a significant increase in the energy stored in the cavities. As a result, 125 W of power passes through the Faraday isolator in the forward direction, and only ~5 W, in the reverse direction. Thus, in the locked state the isolator must block 5 W of laser beam power, while transmitting a total of 130 W.

State A. If for any reason $\Delta\varphi$ changes sharply, the cavity becomes unlocked, which leads to an increase in the power of the light propagating towards the laser source. It is reasonable to examine the most unfavourable case, where $\Delta\varphi$ reaches zero, interference becomes constructive, and the power of the back-propagating light is about four times the laser source power. The stored energy is deposited in the optical isolator and photodetector in ~0.8 ms – the time determined by the fineness and length of the cavities. This time is much shorter than the characteristic temperature equilibration time in optical elements, so heating is a highly unsteady-state process.

Thus, in state A the total laser light power in the isolator increases five times compared to the locked state and the power of the back-propagating light increases one hundred times in a characteristic time of 0.8 ms.

State B. After the stored energy is removed from the cavities as a result of lock loss, the cavities are in the unlocked state. In this state, the beams passing through the Faraday isolator in the two directions have roughly equal powers. This state persists for several minutes, until locking of the interferometer. Thus, the total laser light power in the isolator increases by almost a factor of 2 compared to the locked state, and the power of the back-propagating light increases 25 times.

State C. It is a transient state resulting from locking of and energy storage in the LIGO interferometer. The power of the back-propagating light may increase sharply by chance to 125 W in 1–10 ms. Compared to the locked state, the power of the back-propagating light may increase 25 times. This state is very similar to state B but persists for a shorter time. Therefore, if the isolator ensures necessary isolation in state B, state C presents no hazard to the source. In what follows, we will restrict ourselves to considering regimes A and B.

3. Heating conditions and parameters of the optical isolator

Consider two configurations of Faraday isolators: a classic configuration (Fig. 1a) and one with polarisation distortion compensation (Fig. 1b), both employing [111]-oriented TGG crystals as magneto-optical elements. The absorption in the crystals is weak, so heat release is independent of the (longitudinal) z-coordinate. Linearly polarised beam with a Gaussian transverse intensity profile (1/e diameter of 5 mm) propagates from a laser source to an isolator. A beam with the same intensity profile propagates in the reverse direction and is blocked by the isolator.

The optical surfaces of the magneto-optical elements are located in vacuum. The elements are cooled by a copper tube to reduce the average temperature in the locked state. The

Table 1. Thermal load on the Faraday isolator in different states of the LIGO interferometer.

State	Total laser light power in the isolator/W	Heat generation rate in watts at an absorption coefficient $\varkappa = 10^{-3}$ cm^{-1}	Duration	Back-reflected power/W
In lock	125 + 5 = 130	0.26	infinity	5
A	125 + 500 = 625	1.25	~1 ms	500
B	125 + 125 = 250	0.5	several minutes	125
C	125 + 125 = 250	0.5	1–10 ms	125

heat transfer is a linear process, with a coefficient q near 100 W m^{-2} K^{-1} [20]. The radiative heat transfer (proportional to T^4, where T is the absolute temperature) at the isolator end faces is substantially smaller. The effective radiative heat transfer coefficient can be evaluated by linearising the expression for the power radiated by a black body near 300 K: it does not exceed 7 W m^{-2} K^{-1}.

The parameters of the magneto-optical elements are given below:

Radius/mm	10
Length (classic configuration, one element)/mm	20
Length (configuration with compensation, two elements)/mm	10
Crystal orientation	[111]
Absorption coefficient/cm^{-1}	10^{-3}
Density/kg m^{-3}	7320 [21]
Verdet constant (1064 nm)/rad K^{-1} m^{-1}	−40 [22]
Linear expansion coefficient/K^{-1}	9.4×10^{-6} [5]
Thermal conductivity/W m^{-1} K^{-1}	5 [21]
Index of refraction	1.95 [23]
Specific heat/J kg^{-1} K^{-1}	385±8 [21]
Elasto-optic coefficients:	
p_{11}	0.02
p_{12}	0.08
p_{44}	−0.07
Poisson's ratio	0.22
Young's modulus E/GPa	169 [24]

The coefficients p_{11}, p_{12}, p_{44} are not known with sufficient accuracy, but the above values give adequate results in the plane strain approximation (for both the [111] and [001] orientations) and satisfy the relation $2p_{44}/(p_{11}-p_{12}) \approx 2.3$ [19, 25]. This strongly suggests that the present results are quite reliable. At the same time, the true values of p_{11}, p_{12} and p_{44} may differ markedly from those above.

The time-dependent temperature, the corresponding elastic strain and polarisation distortion of optical pulses were calculated using the code described in Refs [26–29]. In the case of cylindrical symmetry, it allows one to calculate time-dependent temperature distributions in optical elements, the corresponding elastic strain and the strain-induced radiation phase and polarisation distortions in arbitrarily oriented cubic and uniaxial crystals, ceramics and isotropic optical materials.

4. Calculation of optical isolation in the LIGO detector under various thermal conditions

Calculations demonstrate that, during heating with an axisymmetric constant Gaussian heat source, temperature gradients in a magneto-optical element increase monotonically from the instant when heating begins and reach a maximal, time-independent value corresponding to the locked state. The steady-state temperature distribution in an element (at time $t = \infty$) is shown in Fig. 3a. Figures 3b and 3c show the steady-state distributions of the ε_{rr} and ε_{zz} strain tensor components, which correspond to the local depolarisation (Γ) distributions in Figs 4a and 4b for the configurations without and with compensation, respectively. The integrated depolarisation in the configuration without compensation is $\gamma_{nc} = 2.14\times10^{-4}$, and that in the configuration with compensation is $\gamma_c = 2.03\times10^{-9}$. Local and integrated depolarisations are introduced like in Ref. [2] and have the meanings of the normalised intensity and power of the depolarised beam component, respectively. It is worth noting that the topology of the local depolarisation distribution strongly depends on the crystal orientation [19].

In state A, the thermal load power corresponds to exponential energy removal from the cavity with a characteristic time of 0.8 ms starting at time $t = 0$ (Fig. 5).

Calculations demonstrate that the temperature, temperature gradients, and depolarisation in the element reach their maximum values about 5 ms after the onset of state A. The increase in integrated depolarisation is negligible: ~10^{-6} for the configuration without compensation and ~10^{-10} for the configuration with compensation. Thus, the main hazard in state A is that the power of the back-propagating light is increased by a factor of 100.

In state B, the Faraday isolator is heated by two counter-propagating beams of the same power: 125 W. Figure 6 shows the time dependences of integrated depolarisation for the configurations with and without compensation. Like in state A, the main hazard is presented by the sharp increase in the

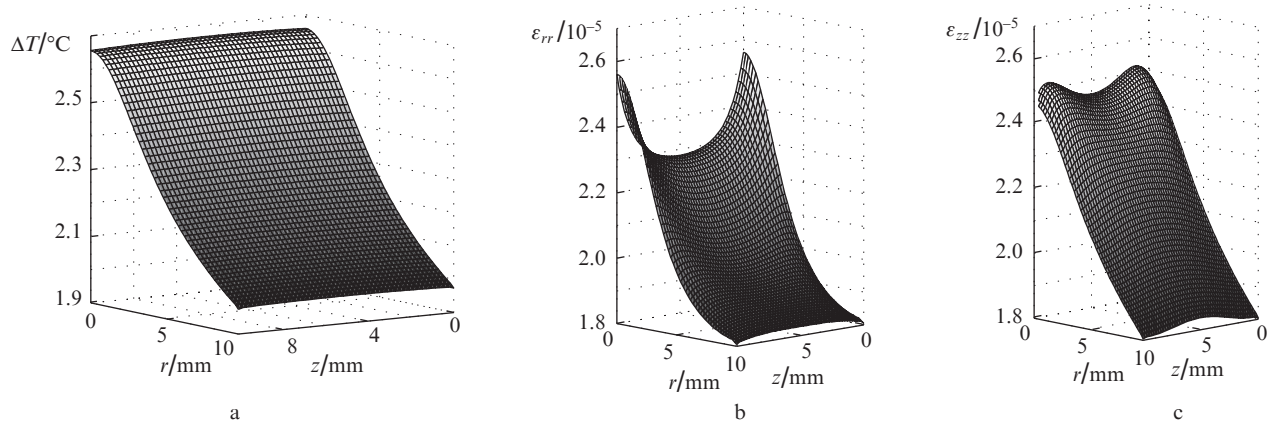

Figure 3. (a) Temperature, (b) ε_{rr} and (c) ε_{zz} distributions in the locked state.

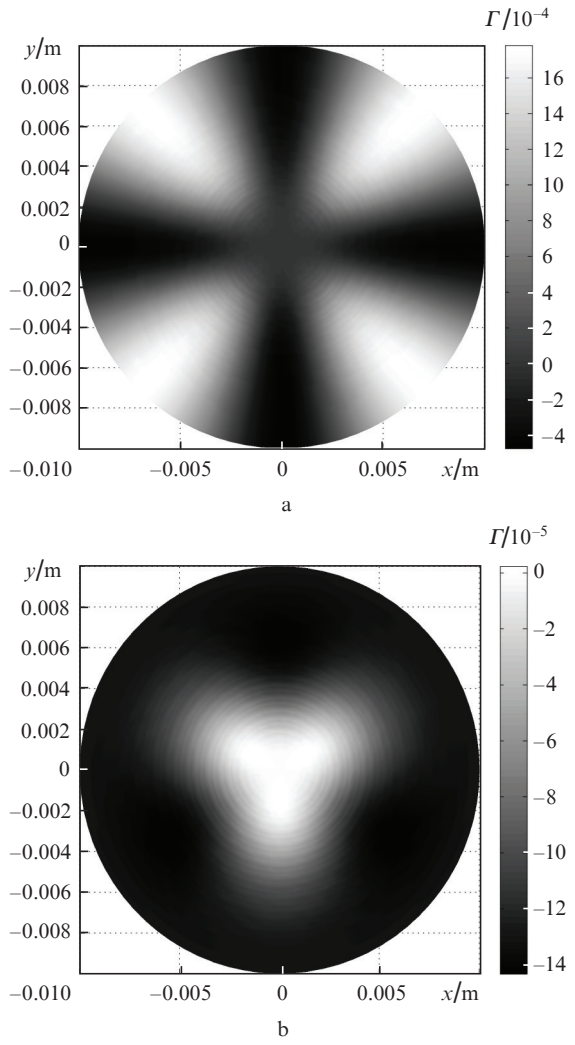

Figure 4. Local depolarisation, σ, for the configurations (a) without and (b) with compensation; [111] crystal orientation.

power of the back-reflected light. In contrast to state A, however, heating is significant, leading to a further gradual reduction in the degree of isolation. It is fair to note that the temperature in the magneto-optical element equilibrates on two timescales. During the first 10 s, the temperature gradients in the specimen reach their steady-state values to within 20%, and their further variation, related to overall heating of the

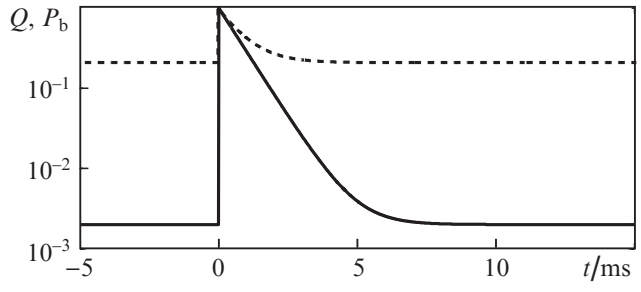

Figure 5. Time dependences of normalised heat release, Q (dashed line), and normalised power of back-propagating light, P_b (solid line), in state A.

element, is much slower. After about 15 min, the integrated depolarisation differs little from its steady-state level: $\gamma_c = 3.7\times10^{-8}$ and $\gamma_{nc} = 7.9\times10^{-4}$.

Since the thermally induced depolarisation in the isolator increases rather slowly, the associated increase in the power of the back-propagating light can be hindered by introducing an additional active isolation of the source, e.g. mechanical or electro-optical. Thus, the peak-power of the light that reaches the source in state B can be reduced by four times in the configuration with compensation and by almost a factor of 18 in that without compensation. The requirements for the response rate of the active isolation of the source can be assessed from Fig. 6.

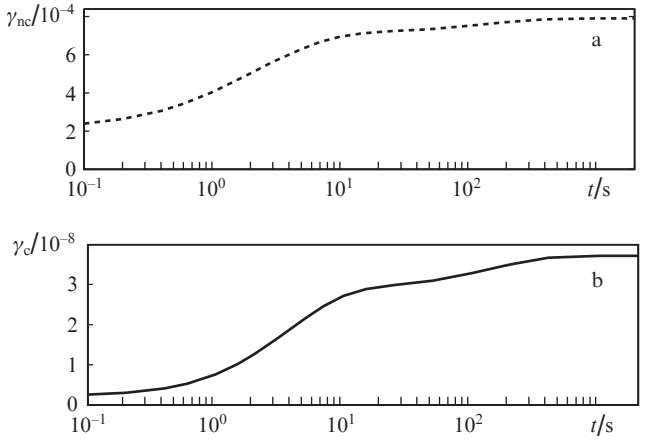

Figure 6. Time dependences of integrated depolarisation for the configurations (a) without and (b) with compensation in state B.

5. Conclusions

To prevent the laser source of the LIGO interferometer from being damaged by the back-propagating light, use is made of a Faraday isolator. We have considered the operation of the isolator in transient states where the power of the light propagating in the backward direction through the isolator may considerable exceed the power of the light propagating in the forward direction, with the associated increase in heat release and reduction in the degree of optical isolation.

Analysis of the transient states of the LIGO interferometer indicates that, in the case of lock loss, the time dependence of the power of the back-propagating light, P_b, has two prominent maxima, which warrant special attention. One maximum may be observed just after lock loss, when the energy stored in the LIGO interferometer is removed in ~0.8 ms. During this time, the temperature distribution in the optical element of the isolator remains almost unchanged, and the increase in P_b is only due to the factor of 100 increase in the power of the light propagating in the backward direction through the isolator.

The other maximum in P_b may be observed in state B and is caused by two factors: the increase in the power of the back-propagating light and the reduction in the degree of isolation because of the thermal depolarisation. If the former component is inertia-free, heating shows up only after some time. Thus, the power of the light incident on the laser source increases sharply by a factor of 25 and then increases gradu-

ally by several times more, in accordance with Fig. 6. The hazard of damage to the laser source in state B can be substantially reduced by decreasing the time the system is in this state through additional active blocking of the light that travels from the isolator to the laser source.

Acknowledgements. This work was supported by the US National Science Foundation (Grant No. UF11253).

References

1. Khazanov E.A., Kulagin O.V., Yoshida S., Tanner D., Reitze D. *IEEE J. Quantum Electron*., **35**, 1116 (1999).
2. Khazanov E.A. *Kvantovaya Elektron*., **26**, 59 (1999) [*Quantum Electron*., **29**, 59 (1999)].
3. Zheleznov D.S., Mukhin I.B., Palashov O.V., Khazanov E.A., Voitovich A.V. *IEEE J. Quantum Electron*., **43**, 451 (2007).
4. Snetkov I.L., Mukhin I.B., Palashov O.V., Khazanov E.A. *Opt. Express*, **19**, 6366 (2011).
5. Khazanov E.A. *Appl. Opt*., **43**, 1907 (2004).
6. Andreev N.F., Katin E.V., Palashov O.V., Potemkin A.K., Reitze D.H., Sergeev A.M., Khazanov E.A. *Kvantovaya Elektron*., **32**, 91 (2002) [*Quantum Electron*., **32**, 91 (2002)].
7. Mukhin I.B., Khazanov E.A. *Kvantovaya Elektron.*, **34**, 973 (2004) [*Quantum Electron*., **34**, 973 (2004)].
8. Kagan M.A., Khazanov E.A. *Appl. Opt*., **43**, 6030 (2004).
9. Voitovich A.V., Katin E.V., Mukhin I.B., Palashov O.V., Khazanov E.A. *Kvantovaya Elektron*., **37**, 471 (2007) [*Quantum Electron*., **37**, 471 (2007)].
10. Khazanov E., Andreev N., Babin A., Kiselev A., Palashov O., Reitze D. *J. Opt. Soc. Am. B*, **17**, 99 (2000).
11. Palashov O.V., Zheleznov D.S., Voitovich A.V., Zelenogorsky V.V., Kamenetsky E.E., Khazanov E.A., Martin R.M., Dooley K.L., Williams L., Lucianetti A., Quetschke V., Mueller G., Reitze D.H., Tanner D.B., Genin E., Canuel B., Marque J., submitted to *J. Opt. Soc. Am. B* (2012).
12. Katherine L., Dooley K., Arain M.A., Feldbaum D., Frolov V.V., Heintze M., Hoak D., Khazanov E.A.,Lucianetti A., Martin R.M., Muller G., Palashov O.V., Quetschke V., Reitze D.H., Savage R., Tanner D.B., Williams L.F., Wu W., accepted in *Rev. Sci. Instrum.* (2012).
13. Kamionkowski M. *Nature*, **460**, 964 (2009).
14. Abbott B. et al. *Nature*, **460**, 990 (2009).
15. Abbott B. et al. *Rep. Prog. Phys*., **72**, 076901 (2009).
16. Accadia T. et al. *J. Phys. Conf. Ser*., **203**, 012074 (2010).
17. Ge T., Lu D., Wu J., Xu K., Lin J. *High Power Laser Part. Beams*, **22**, 1229 (2010).
18. Acernese F. et al. *Appl. Opt*., **47**, 5853 (2008).
19. Khazanov E.A., Andreev N.F., Mal'shakov A.N., Palashov O.V., Poteomkin A.K., Sergeev A.M., Shaykin A.A., Zelenogorsky V.V., Ivanov I., Amin R.S., Mueller G., Tanner D.B., Reitze D.H. *IEEE J. Quantum Electron*., **40**, 1500 (2004).
20. Popov V.M. *Teploobmen v zone kontakta raz'emnykh i neraz'emnykh coedinenii* (Heat Transfer in the Contact Zone of Detachable and Permanent Connections) (Moscow: Energiya, 1971).
21. Chen X., Galemezuk R., Salce B., Lavorel B., Akir C., Rajaonah L. *Solid State Commun.*, **110**, 431 (1999).
22. Raja M.Y.A., Allen D., Sisk W. *Appl. Phys. Lett*., **67**, 2123 (1995).
23. Schlarb U., Sugg B. *Phys. Status Solidi B*, **182**, K91 (1994).
24. Durygin A., Drozd V., Paszkowicz W., Werner-Malento E., Buczko R., Kaminska A., Saxena S., Suchocki A. *Appl. Phys. Lett.*, **95**, 141902 (2009).
25. Khazanov E., Andreev N., Palashov O., Poteomkin A., Sergeev A., Mehl O., Reitze D. *Appl. Opt*., **41**, 483 (2002).
26. Snetkov I.L., Soloviev A.A., Khazanov E.A. *Kvantovaya Elektron.*, **39**, 302 (2009) [*Quantum Electron*., **39**, 302 (2009)].
27. Zelenogorsky V.V., Solovyov A.A., Kozhevatov I.E., Kamenetsky E.E., Rudenchik E.A., Palashov O.V., Silin D.E., Khazanov E.A. *Appl. Opt*., **45**, 4092 (2006).
28. Soloviev A.A., Kozhevatov E.A., Palashov O.V., Khazanov E.A. *Kvantovaya Elektron*., **36**, 939 (2006) [*Quantum Electron*., **36**, 939 (2006)].
29. Soloviev A.A., Khazanov E.A., Kozhevatov I.E., Palashov O.V. *Appl. Opt*., **46**, 3821 (2007).